

A need to revise stellar opacities from asteroseismology of δ Scuti stars

JADWIGA DASZYŃSKA-DASZKIEWICZ,¹ PRZEMYSŁAW WALCZAK,¹ ALEXEY PAMYATNYKH,² WOJCIECH SZEWCZUK,¹ AND
WOJCIECH NIEWIADOMSKI¹

¹*University of Wrocław, Faculty of Physics and Astronomy
Astronomical Institute, ul. Kopernika 11
PL-51-622 Wrocław, Poland*

²*Nicolaus Copernicus Astronomical Center, Polish Academy of Sciences
ul. Bartycka 18, PL-00-716 Warsaw, Poland*

ABSTRACT

We construct seismic models of the four double-mode radial δ Scuti stars adopting opacities from three databases: OPAL, OP and OPLIB. The aim is to find the models that fit the observed frequencies of the two radial modes and have the effective temperature and luminosity consistent with the observed values. Using the Bayesian analysis based on Monte Carlo simulations, we obtain that only the OPAL seismic models are caught within the observed error box in the HR diagram. Seismic models computed with the OP and OPLIB data are much cooler and less luminous. By including the relative amplitude of the bolometric flux variations (the so-called parameter f) into these simulations, we constrain the efficiency of convection in the envelopes, described by the mixing length parameter α_{MLT} . We get $\alpha_{\text{MLT}} \approx 0.5$ for BP Peg, AE UMa and RV Ari (Population I stars) and $\alpha_{\text{MLT}} \approx 1.0$ for SX Phe (Population II star). For all the stars, overshooting from the convective core seems inefficient. A similar effect of opacity should occur also for classical Cepheids or RR Lyr stars that are used as standard candles to measure the universe.

Keywords: Stellar evolution(1599) — Stellar pulsations(1625) — δ Scuti variable stars(370) — Atomic data(2216) — Asteroseismology(73)

1. INTRODUCTION

Asteroseismology provides the most stringent constraints on the theory of stellar structure and evolution. It also offers a test of microphysics data, in particular stellar opacities, which are among the major and still uncertain components of modern astrophysics.

The opacity calculations are almost 100 years old and it seems that their revision is an unfinished story. Extensive opacity calculations that included for the first time bound-bound absorption started in Los Alamos (Cox & Stewart 1962; Cox 1965) and were known as the Los Alamos Opacity Library (LAOL) (Hübner et al. 1977). For many years, these data were widely used but some disagreements were waiting to be explained, e.g., problems with the standard solar model, an unknown mechanism of pulsations in B-type stars, too large period ratios in classical Cepheids models. In the early nineties stellar opacities were recalculated by two independent teams: OPAL (Iglesias et al. 1992; Rogers & Iglesias 1992) and OP (Seaton 1993; Seaton et al. 1994). The most spectacular result was the finding of a local maximum caused by a huge number of transition lines of iron group elements. This maximum occurs at temperature of about 200 000 K and is called the Z-bump.

The discovery of the Z-bump was a big step forward in stellar physics, however there are still some uncertainties and many indications that something is still missing and/or has not been correctly included (Blancard et al. 2016). The first example is a disagreement between the standard solar model and the helioseismic and neutrino-flux predictions (e.g., Turck-Chieze et al. 2004; Guzik 2008; Christensen-Dalsgaard et al. 2009) that arose after the revision of solar

chemical abundances (Asplund et al. 2005, 2009). The laboratory measurements at physical conditions similar to the boundary of the solar convection zone have indicated that the Rosseland mean opacities of iron predicted by all codes are underestimated by 30 to 400 % (Bailey et al. 2015; Pradhan & Nahar 2018; Zhao et al. 2018). The 30–45% underestimate of iron opacity at stellar interior temperatures was also measured by Nagayama et al. (2019). Another example is a presence of high-order gravity modes in β Cephei and δ Scuti stars, that are not excited in standard-opacity models (e.g., Pamyatnykh et al. 2004; Balona 2014). Increasing the mean opacity at temperature of about 290 000 K, where nickel has its maximum contribution to the Z-bump, helped to excite g modes in β Cep models (Salmon et al. 2012; Daszyńska-Daszkiewicz et al. 2017). In the case of δ Scuti stars, an increase of opacity at $T = 115\,000$ K allowed to make g modes unstable (Balona et al. 2015). This new opacity bump at $T = 115\,000$ K was indeed identified by Cugier (2012, 2014) in the Rosseland mean opacities taken from the model atmospheres of Castelli & Kurucz (2003).

Seismic models, that is, models that reproduce the observed frequencies of the identified pulsational modes, are also sensitive to the adopted opacity tables (e.g., Daszyńska-Daszkiewicz et al. 2017, 2020, 2021, 2022). Here, we present this effect for the double-mode radially pulsating δ Sct stars. These pulsators are of special interest because the period ratio of two consecutive radial modes (usually the fundamental and first overtone) takes the value in a very small range. On the other hand, we get the period ratio from space observations with an accuracy of up to six decimal places. We performed extensive seismic studies, based on the Monte Carlo simulations, for the four high-amplitude δ Sct (HADS) stars: BP Peg, AE UMa, RV Ari and SX Phe. The first three stars belong to Population I and the last one, SX Phe, belongs to Population II. One often talks about a separate group of pulsating variables with SX Phe as their prototype.

The remainder of the paper is organized as follows. In Section 2, we explain the motivation for our studies. Section 3 contains the results of seismic modelling for the four HADS stars. The last Section is the summary. Details of seismic modelling with the Bayesian analysis based on the Monte Carlo simulations are given in Appendix.

2. MOTIVATION

Three opacity databases are commonly used in stellar evolution computations: OPAL (Iglesias & Rogers 1996), OP (Seaton 1996, 2005) and OPLIB (Colgan et al. 2015, 2016). There are some subtle differences between these data that result from the adopted physics and methods of computations. However, they have, in general, a minor effect on evolutionary tracks. This is shown in the left panel of Fig. 1, where we plotted the tracks in the Hertzsprung-Russell (HR) diagram, computed for a mass $M = 1.8 M_{\odot}$ with the OPAL, OP and OPLIB opacities. For these tracks, we adopted a typical initial hydrogen abundance by mass $X_0 = 0.70$ and metallicity by mass $Z = 0.014$.

Nevertheless, we found that opacity data has a very significant effect on a frequency ratio of consecutive radial pulsational modes. In the right panel of Fig. 1, we show the corresponding evolution of a frequency ratio of the fundamental and first overtone radial modes. Grey dots represent the models with the same values of the effective temperature $T_{\text{eff}} = 7030$ K and luminosity $\log L/L_{\odot} = 1.2$. We selected these models to present the pure effect of opacity data not blurred by the effect of T_{eff} or $\log L/L_{\odot}$.

Evolutionary computations were performed using the Warsaw-New Jersey code, (e.g., Pamyatnykh 1999). The code takes into account the mean effect of the centrifugal force, assuming solid-body rotation and constant global angular momentum during evolution. All the stars analysed in this paper are slow rotators, which is one of the main properties of HADS stars. Therefore, the effect of differential rotation will be negligible.

The treatment of convection in the stellar envelope relies on the standard mixing-length theory (MLT) and the efficiency of convection is described by the mixing length parameter α_{MLT} . At lower temperature range, i.e., for $\log T < 3.95$, opacity data from Ferguson et al. (2005) were used. The solar chemical mixture was adopted from Asplund et al. (2009) and the OPAL2005 equation of state was used (Rogers et al. 1996; Rogers & Nayfonov 2002). The evolutionary tracks in Fig. 1 were computed at zero-rotation and for $\alpha_{\text{MLT}} = 0.5$, to focus only on the opacity effect.

Stellar pulsations were computed using linear non-adiabatic code of Dziembowski (1977). This code adopts the frozen convection approximation, i.e., the convective flux does not change during the pulsations, which is a reasonable approach if convection is not very efficient in the envelope. The effects of rotation on pulsational frequencies are taken into account up to the second order in the framework of perturbation theory. In the case of radial modes, the second order effects of rotation reduces to the factor $4\nu_{\text{rot}}^2/3\nu_{\text{puls}}$ independently of the radial order n (e.g., Simon 1969; Kjeldsen et al. 2018), where ν_{rot} is the frequency of rotation. At a rotation rate of $18 \text{ km}\cdot\text{s}^{-1}$, for the dominant

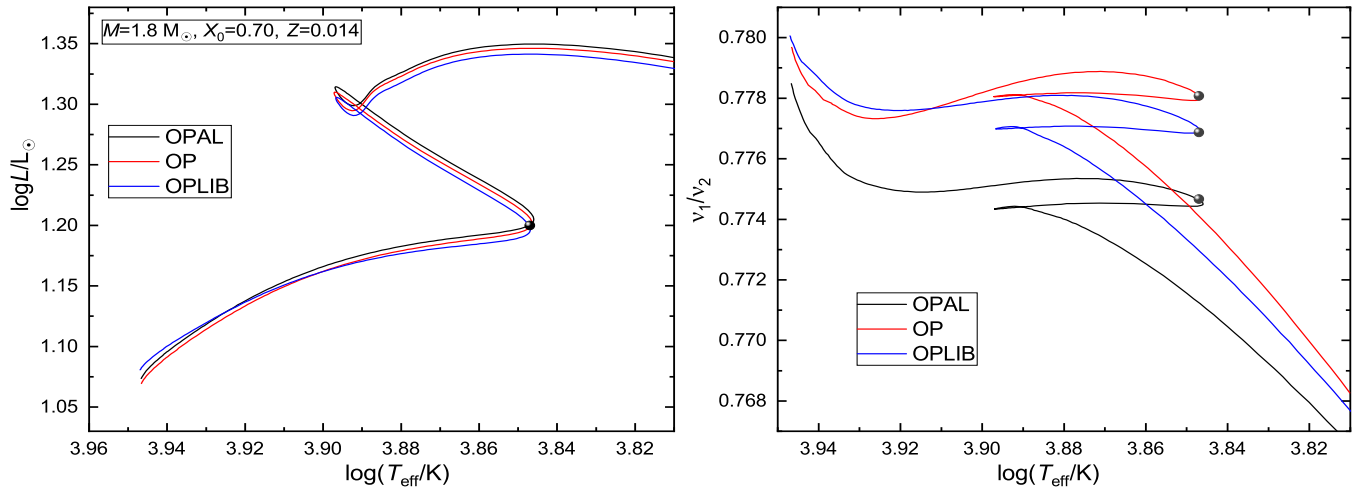


Figure 1. Left panel: evolutionary tracks of a $1.8 M_{\odot}$ star computed with the OPAL, OP and OPLIB opacity tables. Right panel: the evolution of a frequency ratio of the fundamental and first overtone radial modes. Grey dots represent models with the effective temperature, $T_{\text{eff}} = 7020$ K, and luminosity, $\log L/L_{\odot} = 1.2$, marked with a dot on the left panel.

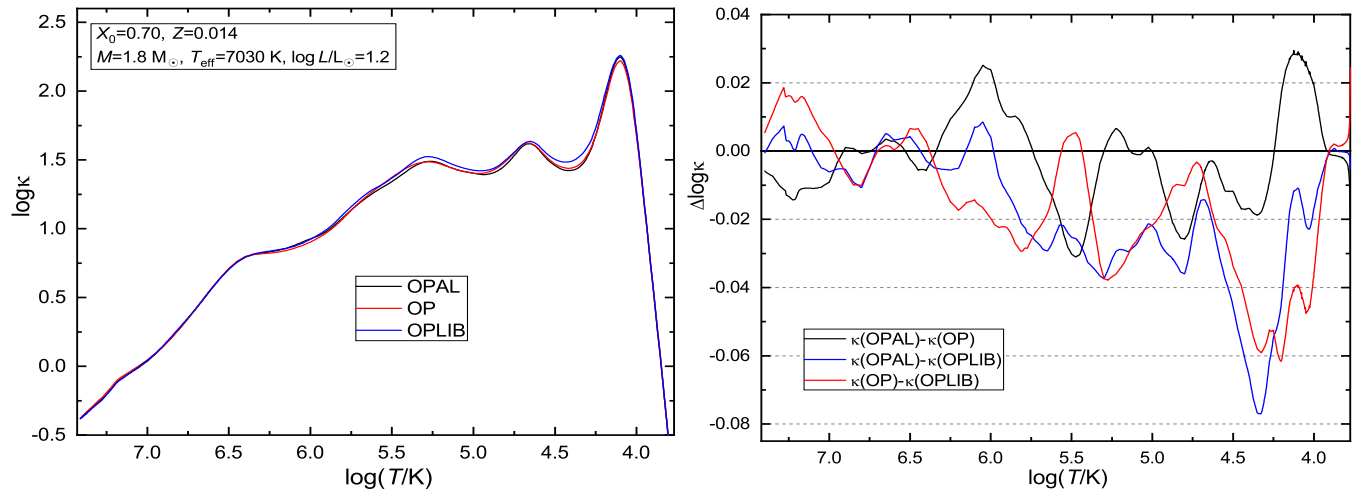


Figure 2. Left panel: the run of the Rosseland mean opacity from OPAL, OP and OPLIB data inside the model with a mass $1.8 M_{\odot}$, effective temperatures $T_{\text{eff}} = 7030$ K and luminosity $\log L/L_{\odot} = 1.2$. Right panel: the corresponding differences in $\log \kappa$.

frequencies of the studied stars, this factor amounts to about 0.004 d^{-1} in the case of SX Phe and about 0.002 d^{-1} in the case of other three HADS stars. For higher frequencies these values will be smaller.

For the models marked with grey dots in Fig. 1, we plotted in Fig. 2 the run of the Rosseland mean opacity. As mentioned, all three models have the same effective temperature $T_{\text{eff}} = 7030$ K and luminosity $\log L/L_{\odot} = 1.2$. As one can see the overall run of $\log \kappa(T)$ from the three databases is very similar. However, by drawing the differences, it is possible to locate certain depths where three opacity profiles deviate from each other. This is shown in the right panel of Fig. 2. For example, there are significant differences between OPAL, OP and OPLIB around temperature corresponding to the hydrogen and first helium ionization ($\log T \approx 4.0 - 4.45$). On the other hand, all three κ 's are very close in the second helium ionization zone ($\log T \approx 4.67$), where main driving of pulsations for δ Sct stars occurs. One can also see that OPAL and OP are very close to each other near the Z-bump, i.e., near $\log T = 5.2 - 5.3$. Instead, the data from OP and OPLIB are very similar near $\log T \approx 5.46$, where nickel has its maximum contribution to the opacity around Z-bump.

All these small differences in opacity tables (of a few percent) cause huge differences in the frequency ratio, already in the third decimal place, while modern observations give accuracy down to six decimal places. In the next section, we will study how these differences affect seismic models of the realistic stars.

Table 1. The main parameters from observations of the four studied δ Sct stars, i.e., the range of effective temperature, luminosity, metallicity and the projected rotational velocity.

star	Pop.	T_{eff} [K]	$\log L/L_{\odot}$	[m/H] [dex]	$V_{\text{rot}} \sin i$ [km·s ⁻¹]
BP Peg	I	6800–8100	1.247(120)	0.2	~18
AE UMa	I	7100–8200	1.091(90)	-0.3	<10
RV Ari	I	7000–8200	1.103(26)	0.1	~18
SX Phe	II	7000–8600	0.899(17)	-1.0	18(2)

Table 2. Frequencies of the fundamental (ν_1) and first overtone (ν_2) radial modes of the four studied HADS stars. The frequencies of BP Peg were derived from the ASAS data and their amplitudes are given in [mmag]. For the other three stars the frequencies were obtained from the TESS light curves and the amplitudes are expressed in [ppt].

star	ν_1 [d ⁻¹]	Ampl.	ν_2 [d ⁻¹]	Ampl.	ν_1/ν_2
BP Peg	9.128797(4)	208(4)	11.83315(3)	34(4)	0.77146
AE UMa	11.625598(2)	131.65(2)	15.031250(5)	30.70(2)	0.77343
RV Ari	10.737888(55)	128.84(3)	13.899137(121)	39.62(2)	0.77256
SX Phe	18.193566(3)	133.64(1)	23.379306(7)	32.92(10)	0.77819

3. SEISMIC MODELS OF THE FOUR HIGH-AMPLITUDE δ SCUTI PULSATORS

To study the effect of opacity, we selected four high-amplitude δ Sct stars: BP Pegasi, AE Ursa Majoris, RV Arietis and SX Phoenicis. These are relatively simple objects because: 1) they pulsate in the two radial modes: fundamental and first overtone, 2) the linear theory of pulsations is still applicable, because even in the case of classical Cepheids, which have the light amplitudes about five times larger, nonlinear period ratios differ from linear values only by several tenths of a per cent (e.g., Kollath & Buchler 2001). 3) they are very slow rotators, 4) their effective temperatures are not low enough for convection in their envelopes to be efficient, 5) mass loss can be neglected, and 6) there are no observational evidences for anomalous surface abundances, so in the first approximation the effect of diffusive settling or radiative levitation can be safely neglected.

Some results for SX Phe and BP Peg were already presented in Daszyńska-Daszkiewicz et al. (2020) and Daszyńska-Daszkiewicz et al. (2022), respectively. Here, we included the Monte Carlo simulations for SX Phe and increased the number of simulations for BP Peg.

The basic parameters of the studied stars are given in Table 1. The range of the effective temperature were gathered from the literature and luminosity were derived from the Gaia DR3 data (Gaia Collaboration et al. 2022) in this paper. This T_{eff} range also includes the changes due to pulsations. The last two columns contain the metallicity [m/H] and projected rotational velocities $V_{\text{rot}} \sin i$. These parameters were adopted from Rodriguez et al. (1992) for BP Peg, AE UMa and RV Ari, and from Antoci et al. (2019) for SX Phe.

In Table 2, we list the observed frequencies of the two radial modes and the corresponding amplitudes. In the case of BP Peg, we performed the frequency analysis using the ASAS photometry (Pojmanski 1997). For the other three stars TESS observations were available and we used them to determine the frequencies. We know that in each case these two frequencies are radial modes, based on the period ratio and on the independent mode identification from multi-colour photometry (Daszyńska-Daszkiewicz et al. 2020, 2022, 2023).

Having the two radial modes, fundamental and first overtone, we constructed seismic models that fit the observed frequencies within the errors. Besides, we fitted also the non-adiabatic parameter f for the dominant frequency. This parameter is a relative amplitude of radiative flux variations at the level of the photosphere. The theoretical value of f for a given pulsational mode is derived in the framework of non-adiabatic theory of stellar pulsations and it is complex because there is a phase shift between the flux and radius variations. In the case of δ Sct models, the parameter f is very sensitive to the adopted value of α_{MLT} (e.g., Daszyńska-Daszkiewicz et al. 2003). Therefore, from matching the theoretical and empirical values of f it is possible to get reliable constraints on the efficiency of convection in sub-photospheric layers. The empirical values of f are derived from the photometric amplitudes and phases in at least three passbands, see Daszyńska-Daszkiewicz et al. (2020, 2021, 2022) for recent results.

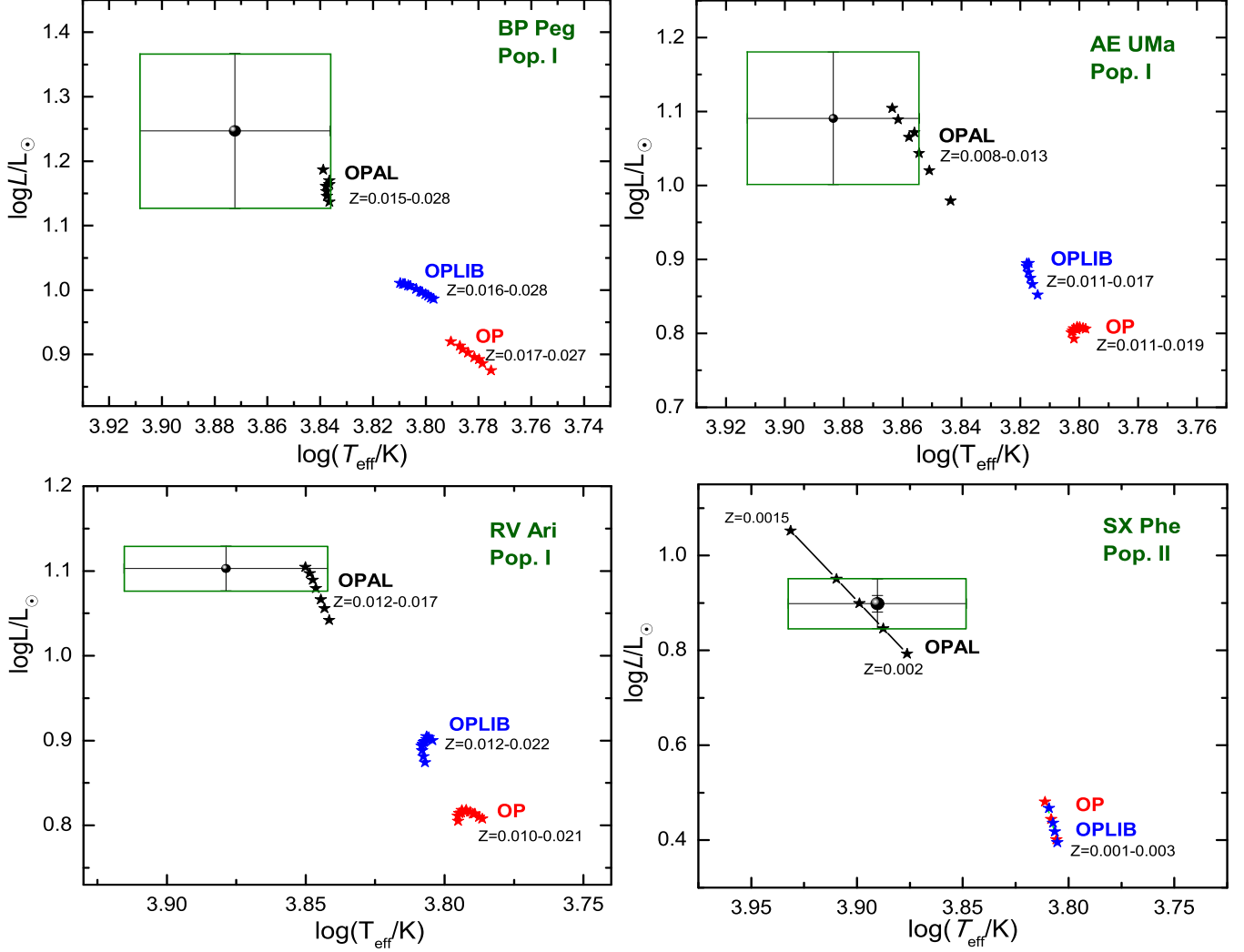


Figure 3. Seismic models of BP Peg, AE UMa, RV Ari and SX Phe constructed with the three opacity data: OPAL, OP and OPLIB. The initial hydrogen abundance by mass was $X_0 = 0.70$ and the range of metallicity Z is given in each case.

Our extensive, complex seismic modelling was made using the Bayesian analysis based on the Monte Carlo simulations. As a result, we obtained constraints on the mass M , metallicity Z , initial hydrogen abundance X_0 , rotational velocity V_{rot} as well as on the mixing length parameter (α_{MLT}). In the case of BP Peg, AE UMa and RV Ari (Population I stars), we got $\alpha_{\text{MLT}} \approx 0.6, 0.4, 0.5$, respectively, and in the case of SX Phe (the Population II star), we obtained $\alpha_{\text{MLT}} \approx 1.0$. Details of our computations and detailed results are given in the Appendix.

Results for $X_0 = 0.70$ and some range of Z are presented in Fig. 3 in the HR diagram. As one can see, in the case of each star, only the OPAL seismic models have effective temperatures and luminosities consistent with the observational determinations. The OP and OPLIB seismic models have far too low values of $\log T_{\text{eff}}$ and $\log L/L_{\odot}$. In the case of the Population I stars, the OP models have parameters even lower than the OPLIB models. In the case of SX Phe, the OP and OPLIB seismic models are in the same position in the HR diagram. All depicted models, for each set of opacity data, are in the post-main sequence phase of evolution. The vast majority of them burn hydrogen in the shell surrounding the core and just one or two models are in the phase of an overall contraction. All seismic models in the main sequence phase of evolution had much too low T_{eff} and $\log L/L_{\odot}$ in the case of each opacity tables. Both radial modes, fundamental and first overtone, are unstable.

4. SUMMARY

We presented the results of extensive seismic modelling for the four high-amplitude δ Sct stars that pulsate in two radial modes, i.e. BP Peg, AE UMa, RV Ari and SX Phe. To this aim we used the Bayesian analysis based on the

Monte Carlo simulations. Three opacity tables were adopted: OPAL, OP and OPLIB. Besides frequencies, we fitted also the parameter f for the dominant frequency in order to constrain, in particular, the mixing length parameter α_{MLT} in the envelope. We obtained $\alpha_{\text{MLT}} \approx 0.6, 0.4, 0.5$ for BP Peg AE UMa and RV Ari, respectively, and $\alpha_{\text{MLT}} \approx 1.0$ for SX Phe.

In the case of each studied HADS, only the OPAL seismic models are close to or within the error box on the HR diagram whereas the OP and OPLIB seismic models are far beyond. This "seismic opacity" discrepancy is independent of the metallicity as it was obtained for stars with different values of $[m/H]$ and even for a Population II HADS SX Phe. Thus, we have shown that there are systematic differences in seismic models of double-mode radial δ Sct pulsators, computed with different opacity data. However, the solution to this puzzle is rather beyond our ability. Rather, this is one more message to atomic physicists that something is still missing in stellar opacities. This is also a warning to those who model double-mode classical Cepheids or RR Lyr stars. Such huge effect of opacity can occur also for these variables which are used as standard candles to measure distances.

The work was financially supported by the Polish National Science Centre grant 2018/29/B/ST9/02803. Calculations have been partly carried out using resources provided by Wroclaw Centre for Networking and Supercomputing (<http://www.wcss.pl>), grant No. 265. This work has made use of data from the European Space Agency (ESA) mission *Gaia* (<https://www.cosmos.esa.int/gaia>), processed by the *Gaia* Data Processing and Analysis Consortium (DPAC, <https://www.cosmos.esa.int/web/gaia/dpac/consortium>). Data collected by the TESS mission and ASAS project were used. Funding for the TESS mission is provided by the NASA's Science Mission Directorate.

REFERENCES

- Antoci, V., Cunha, M. S., Bowman, D. M., & et al. 2019, MNRAS, 490, 4040
- Asplund, M., Grevesse, N., & Sauval, A. J. 2005, in ASP Conference Series, Vol. 336, Cosmic Abundances as Records of Stellar Evolution and Nucleosynthesis in honor of David L. Lambert, 25
- Asplund, M., Grevesse, N., Sauval, A. J., & Scott, P. 2009, ARA&A, 47, 481
- Bailey, J. E., Nagayama, T., Loisel, G. P., & et al. 2015, Nature, 517, 56
- Balona, L. 2014, MNRAS, 437, 1476
- Balona, L., Daszyńska-Daszkiewicz, J., & Pamyatnykh, A. A. 2015, MNRAS, 452, 3073
- Blancard, C., Colgan, J., Cosse, P., & et al. 2016, PhRvL, 117, 249501
- Canuto, V. M., Goldman, I., & Mazzitelli, I. 1996, ApJ, 473, 550
- Castelli, F., & Kurucz, R. L. 2003, in Proceedings of the 210th IAU Symposium, Vol. 210, Modelling of Stellar Atmospheres., 20
- Christensen-Dalsgaard, J., Di Mauro, M. P., Houdek, G., & Pijpers, F. 2009, A&A, 494, 205
- Colgan, J., Kilcrease, D. P., Magee, N. H., & et al. 2015, High Energy Density Physics, 14, 33
- . 2016, ApJ, 817, 116
- Cox, A. N. 1965, in in Aller L. H., MacLauglin D. B., eds, Stellar Structure. Univ. Chicago Press, Chicago, 195
- Cox, A. N., & Stewart, J. N. 1962, AJ, 67, 113
- Cugier, H. 2012, A&A, 547, 42
- . 2014, A&A, 565, 76
- da Silva, L., Girardi, L., Pasquini, L., et al. 2006, A&A, 458, 609, doi: [10.1051/0004-6361:20065105](https://doi.org/10.1051/0004-6361:20065105)
- Daszyńska-Daszkiewicz, J., Dziembowski, W. A., & Pamyatnykh, A. A. 2003, A&A, 407, 999
- Daszyńska-Daszkiewicz, J., Pamyatnykh, A. A., Walczak, P., & et al. 2017, MNRAS, 466, 2284
- . 2021, MNRAS, 505, 88
- Daszyńska-Daszkiewicz, J., Pamyatnykh, A. A., Walczak, P., & Szewczuk, W. 2020, MNRAS, 499, 3034
- . 2022, MNRAS, 512, 3551
- Daszyńska-Daszkiewicz, J., Walczak, P., Szewczuk, W., & Niewiadomski, W. 2023, in preparation
- Dziembowski, W. A. 1977, AcA, 27, 95
- Ferguson, J. W., Alexander, D. R., Allard, F., & et al. 2005, ApJ, 623, 585
- Gaia Collaboration, Vallenari, A., Brown, A. G. A., & et al. 2022
- Guzik, J. A. 2008, Mem.S.A.It., 79, 481
- Heiter, U., Kupka, F., van't Veer-Menneret, C., & et al. 2002, A&A, 392, 619
- Hübner, W. F., Merts, A. L., Magee, N. H., & Argo, M. E. 1977, Los Alamos Report
- Iglesias, C. A., & Rogers, F. J. 1996, ApJ, 464, 943
- Iglesias, C. A., Rogers, F. J., & Wilson, B. G. 1992, ApJ, 397, 717

- Jiang, C., & Gizon, L. 2021, *Research in Astronomy and Astrophysics*, 21, 226
- Jørgensen, B. R., & Lindegren, L. 2005, *A&A*, 436, 127
- Kjeldsen, H., Arentoft, T., & Bedding, T. e. 2018, in *ESA*, 385
- Kollath, Z., & Buchler, R. J. 2001, in *Astrophysics and space science library*, Vol. 257, *Stellar pulsation - nonlinear studies*, 29–60
- Nagayama, T., Bailey, J. E., Loisel, G. P., & et al. 2019, *PhRvL*, 122, 235001
- Pamyatnykh, A. A. 1999, *AcA*, 49, 119
- Pamyatnykh, A. A., Handler, G., & Dziembowski, W. A. 2004, *MNRAS*, 350, 1022
- Pojmanski, G. 1997, *AcA*, 47, 467
- Pradhan, A. K., & Nahar, S. N. 2018, in *ASP Conference Series*, Vol. 515, *Workshop on Astrophysical Opacities*, 79
- Rodrigues, T. S., Bossini, D., Miglio, A., et al. 2017, *MNRAS*, 467, 1433, doi: [10.1093/mnras/stx120](https://doi.org/10.1093/mnras/stx120)
- Rodriguez, E., Rolland, A., Lopez de Coca, P., Garcia-Lobo, E., & Sedano, J. L. 1992, *A&AS*, 93, 189
- Rogers, F. J., & Iglesias, C. A. 1992, *ApJS*, 79, 507
- Rogers, F. J., & Nayfonov, A. 2002, *ApJ*, 576, 1064
- Rogers, F. J., Swenson, F. J., & Iglesias, C. A. 1996, *ApJ*, 456, 902
- Rolland, A., Rodriguez, E., Lopez de Coca, P., & et al. 1991, *A&A Suppl.*, 91, 347
- Salmon, S., Montalbán, J., Morel, T., & et al. 2012, *MNRAS*, 422, 3460
- Seaton, M. J. 1993, in *ASP Conference Series*, Vol. 40, *Inside the Stars*, *IAU Coll.* 137, 222
- Seaton, M. J. 1996, *MNRAS*, 279, 95
- . 2005, *MNRAS*, 362, L1
- Seaton, M. J., Yu Yan, Mihalas, D., & Pradhan, A. K. 1994, *MNRAS*, 266, 805
- Simon, R. 1969, *A&A*, 2, 390
- Turck-Chieze, S., Couvidat, S., Piau, L., & et al. 2004, *PhRvL*, 93, 211102
- Zhao, L., Eissner, W., Nahar, S. N., & Pradhan, A. K. 2018, in *ASP Conference Series*, Vol. 515, *Workshop on Astrophysical Opacities*, 89

APPENDIX

A. ASTEROSEISMIC MODELLING WITH MONTE CARLO-BASED BAYESIAN ANALYSIS

We computed extensive grids of seismic models for each star and employed Monte Carlo-based Bayesian analysis to obtain constraints on various parameters. The analysis was based on the Gaussian likelihood function defined as (e.g., Jørgensen & Lindgren 2005; da Silva et al. 2006; Rodrigues et al. 2017; Jiang & Gizon 2021)

$$\mathcal{L}(E|\mathbf{H}) = \prod_{i=1}^n \frac{1}{\sqrt{2\pi\sigma_i^2}} \cdot \exp\left(-\frac{(\mathcal{O}_i - \mathcal{M}_i)^2}{2\sigma_i^2}\right), \quad (\text{A1})$$

where \mathbf{H} is the hypothesis that represents adjustable model and theory parameters that in case of studied stars were: mass M , initial hydrogen abundance X_0 , metallicity Z , initial rotational velocity $V_{\text{rot},0}$, convective overshooting parameter α_{ov} and the mixing length parameter α_{MLT} . The evidence E represents the calculated observables \mathcal{M}_i , that can be directly compared with the observed parameters \mathcal{O}_i determined with the errors σ_i .

Here, we used the following observations: effective temperature T_{eff} , luminosity L/L_{\odot} , the frequencies of the two radial modes ν_1 and ν_2 , and the non-adiabatic parameter f for the dominant mode. The second mode ν_2 had too low amplitudes to make use of it. To derive the empirical values of f we applied the method of Daszyńska-Daszkiewicz et al. (2003). To this aim, we used the amplitude and phases in the four Strömgren passbands from Rodriguez et al. (1992) for BP Peg, AE UMa and RV Ari, and from Rolland et al. (1991) for SX Phe. The method requires also the model atmospheres and here we relied on Vienna (NEMO) models Heiter et al. (2002) that include turbulent convection treatment from Canuto et al. (1996).

Then, we made a huge number of simulations (from about 90 000 to 160 000 depending on the star) to maximize the likelihood function given in Eq. (A1) in order to constrain the parameters for each star. For each randomly selected set of parameters (M , X_0 , Z , $V_{\text{rot},0}$, α_{ov} and α_{MLT}), we calculated evolutionary and pulsational models.

In the case of the initial hydrogen abundance X_0 , we assumed a beta function $B(2, 2)$ as a prior probability, since we wanted to limit its value to the reasonable range, i.e., from 0.65 to 0.75 with $X_0 = 0.7$ as the most probable. For other parameters we used uninformative priors, i.e., a uniform distribution. Moreover, already first simulations showed that overshooting for the convective core is ineffective because in all runs the parameter α_{ov} tended to zero very fast and did not change. This is because all models with $\alpha_{\text{ov}} > 0$ had much too low values of $\log L/L_{\odot}$. Therefore, we set $\alpha_{\text{ov}} = 0.0$ in further computations.

B. CONSTRAINTS ON PARAMETERS

The most important result of our seismic modeling is that only with the OPAL opacity tables, we were able to match all observables for each star. In the case of OP and OPLIB data, it was often difficult to find any model that reproduced both frequencies and the non-adiabatic f for the dominant mode. Even if such models were found, they were far beyond the error box in the HR diagram.

The results of our simulations with the OPAL data for all studied stars are presented as histograms. The histograms were normalised to 1.0 by the number of all models, thus the numbers on the Y-axis times 100 are the percentage of models with a given parameter range. In Fig. 4, there are shown histograms for masses of BP Peg, AE UMa, RV Ari and SX Phe. The next Figures 5–8, present histograms for Z , X_0 , the current value of rotation V_{rot} and for α_{MLT} . The expected values of the parameters from these distributions as well as of the initial rotation, effective temperature and luminosity are given in Table 3. The errors in parentheses are standard deviations. The current value of rotation V_{rot} corresponds to the given seismic model. In Table 4, we give the median values for the determined parameters. This statistic is more informative for skewed distributions or distributions with outliers, which is the case for some parameters. For example, in the case of BP Peg, AE UMa and RV Ari, rather an upper limit may be given for the rotational velocity. One can see also the asymmetry for the metallicity Z in the case of BP Peg, AE UMa and RV Ari, while the histogram of Z for SX Phe shows quite a symmetric distribution. On the other hand, the histograms for the mixing parameter α_{MLT} are almost symmetric for BP Peg, AE UMa and RV Ari, while in the case of SX Phe we have some skewness. The errors in Table 4 were calculated as the 0.84-quantile minus the median and the median minus the 0.16-quantile. These quantiles correspond to estimates of values separated by one standard deviation from the mean value in the case of a normal distribution.

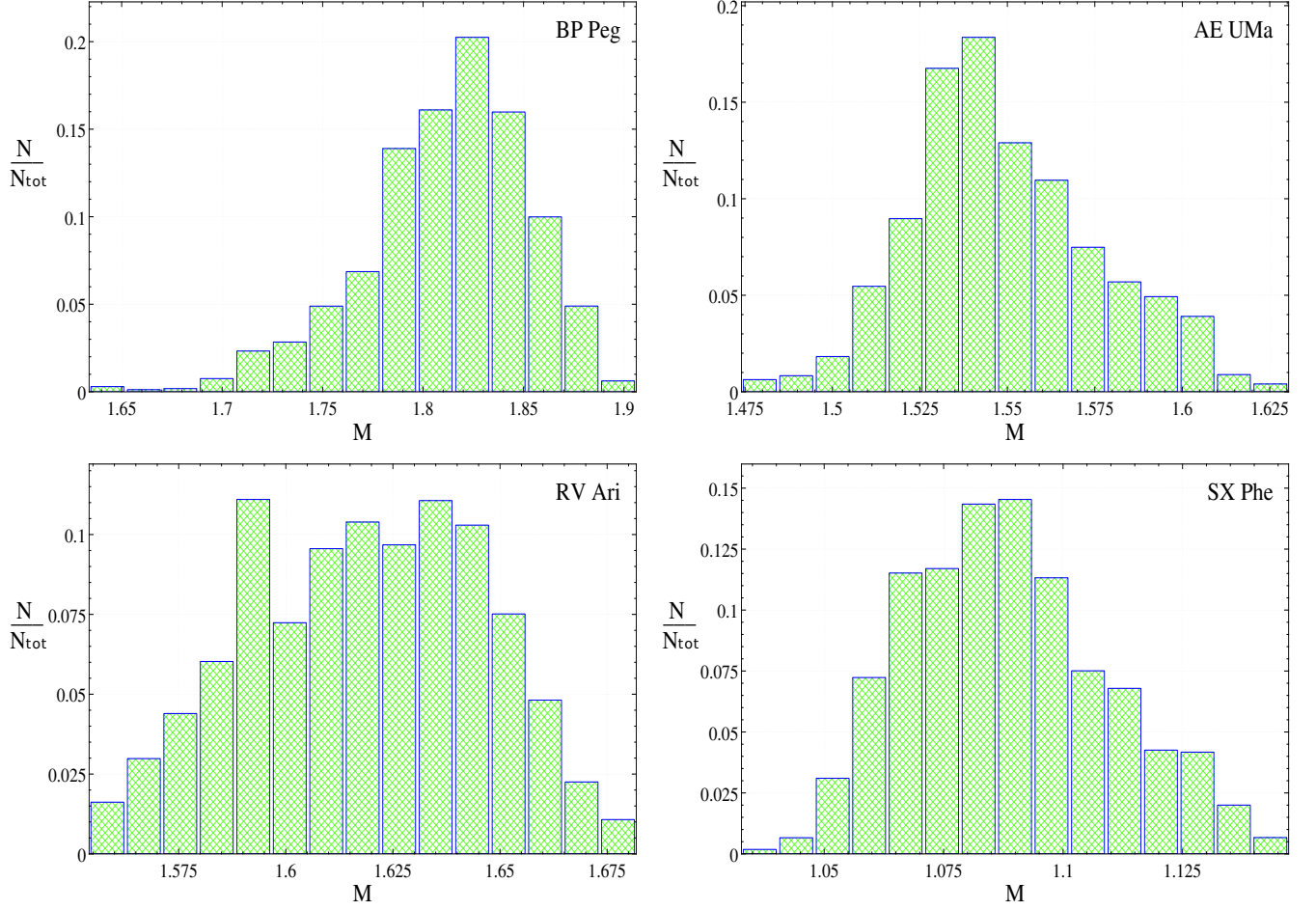


Figure 4. The normalized histograms for the mass (in M_{\odot}) of BP Peg, AE UMa, RV Ari and SX Phe. All seismic models were computed with the OPAL opacities.

Table 3. The expected values of the parameters of the four studied δ Sct stars from the Monte-Carlo simulations. The uncertainties were calculated as the square roots of the variance. Seismic models were computed with the OPAL opacities.

star	M [M_{\odot}]	Z	X_0	α_{MLT}	$V_{\text{rot},0}$ [$\text{km}\cdot\text{s}^{-1}$]	V_{rot} [$\text{km}\cdot\text{s}^{-1}$]	$\log(T_{\text{eff}}/\text{K})$	$\log L/L_{\odot}$
BP Peg	1.81(4)	0.0281(25)	0.682(19)	0.63(7)	16.0(9.3)	15.1(8.8)	3.8353(16)	1.161(10)
AE UMa	1.55(3)	0.0136(7)	0.687(11)	0.43(14)	19.2(11.9)	19.2(11.9)	3.8608(36)	1.085(18)
RV Ari	1.62(3)	0.0168(9)	0.690(9)	0.52(5)	18.(9.3)	17.6(9.2)	3.8494(22)	1.096(12)
SX Phe	1.088(21)	0.00199(5)	0.677(14)	1.04(58)	12.1(7.5)	14.1(8.7)	3.8986(37)	0.889(17)

In the case of each star, all presented models are in the post-main sequence phase of evolution, mostly during the hydrogen-shell burning and very rare in the overall contraction. Main sequence models had always too low effective temperatures and luminosities. Efficiency of convection in the envelopes of the Population I stars, parameterized by α_{MLT} , is rather low and amounts to about 0.5. In the case of SX Phe, which is a lower-mass star and belongs to Population II, convection is more efficient and $\alpha_{\text{MLT}} \approx 1.0$.

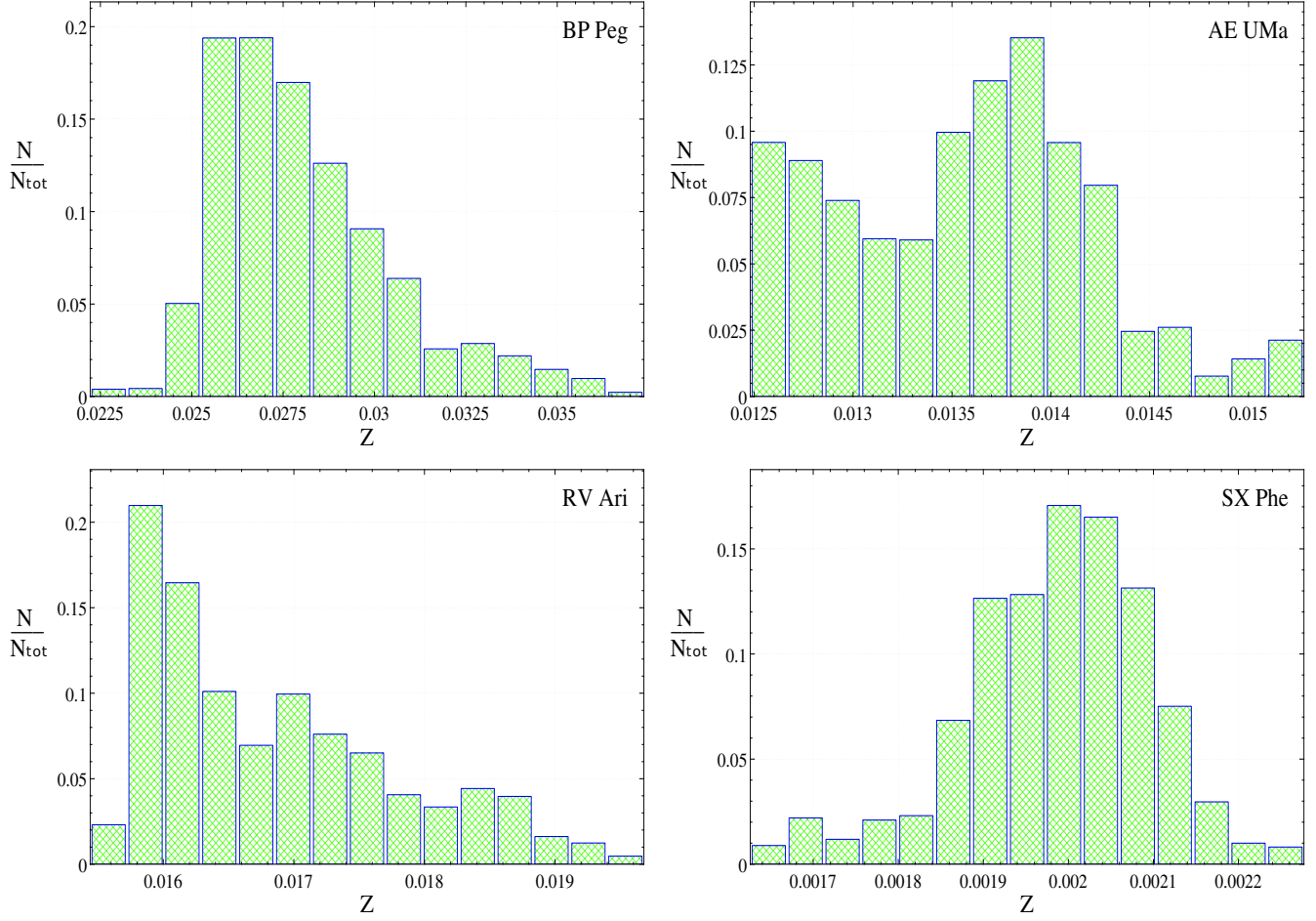


Figure 5. The normalized histograms for the metallicity Z for seismic models computed with the OPAL opacities.

Table 4. The median values of the parameters of the four studied δ Sct stars from the Monte-Carlo simulations. The uncertainties were calculated from quantiles 0.84 and 0.16. Seismic models were computed with the OPAL opacities.

star	M [M_{\odot}]	Z	X_0	α_{MLT}	$V_{\text{rot},0}$ [$\text{km}\cdot\text{s}^{-1}$]	V_{rot} [$\text{km}\cdot\text{s}^{-1}$]	$\log(T_{\text{eff}}/\text{K})$	$\log L/L_{\odot}$
BP Peg	$1.81^{+0.03}_{-0.04}$	$0.0271^{+0.0028}_{-0.0018}$	$0.682^{+0.015}_{-0.023}$	$0.60^{+0.07}_{-0.06}$	$14.9^{+9.8}_{-11.5}$	$14.1^{+9.1}_{-10.9}$	$3.8351^{+0.0013}_{-0.0018}$	$1.158^{+0.010}_{-0.009}$
AE UMa	$1.54^{+0.03}_{-0.02}$	$0.0135^{+0.0006}_{-0.0008}$	$0.685^{+0.012}_{-0.011}$	$0.40^{+0.13}_{-0.14}$	$17.0^{+13.4}_{-12.9}$	$17.0^{+13.5}_{-12.9}$	$3.8606^{+0.0028}_{-0.0043}$	$1.082^{+0.017}_{-0.019}$
RV Ari	$1.62^{+0.03}_{-0.03}$	$0.0164^{+0.0013}_{-0.0007}$	$0.689^{+0.008}_{-0.010}$	$0.51^{+0.05}_{-0.05}$	$16.8^{+9.1}_{-10.9}$	$16.4^{+9.0}_{-10.6}$	$3.8489^{+0.0020}_{-0.0023}$	$1.092^{+0.013}_{-0.010}$
SX Phe	$1.083^{+0.024}_{-0.020}$	$0.00197^{+0.00010}_{-0.00011}$	$0.672^{+0.016}_{-0.012}$	$0.92^{+0.64}_{-0.63}$	$11.0^{+7.8}_{-8.5}$	$12.8^{+9.1}_{-10.0}$	$3.8973^{+0.0040}_{-0.0032}$	$0.884^{+0.019}_{-0.014}$

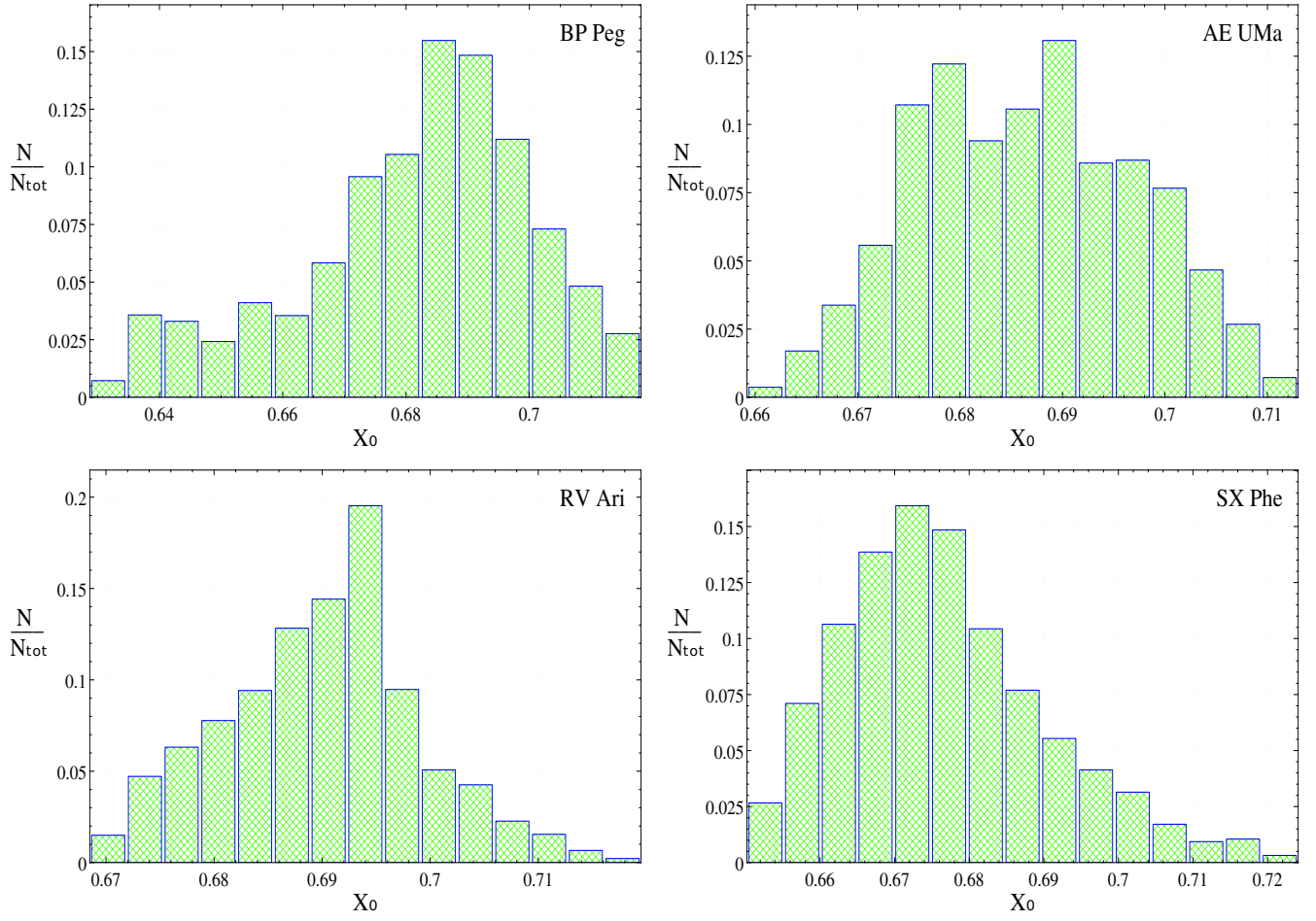


Figure 6. The normalized histograms for the initial hydrogen abundance X_0 for seismic models computed with the OPAL opacities.

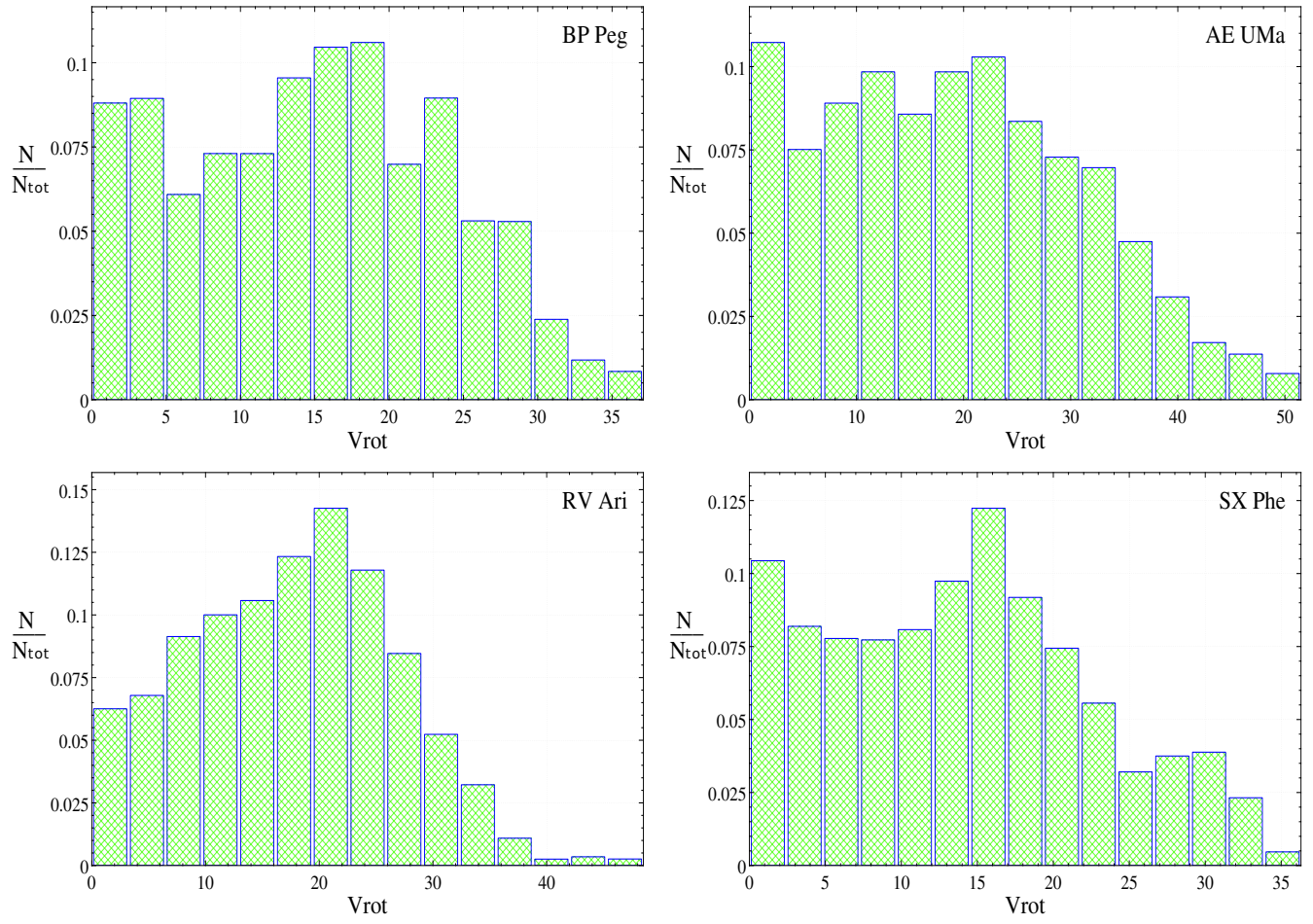


Figure 7. The normalized histograms for the current rotational velocity V_{rot} for seismic models computed with the OPAL opacities.

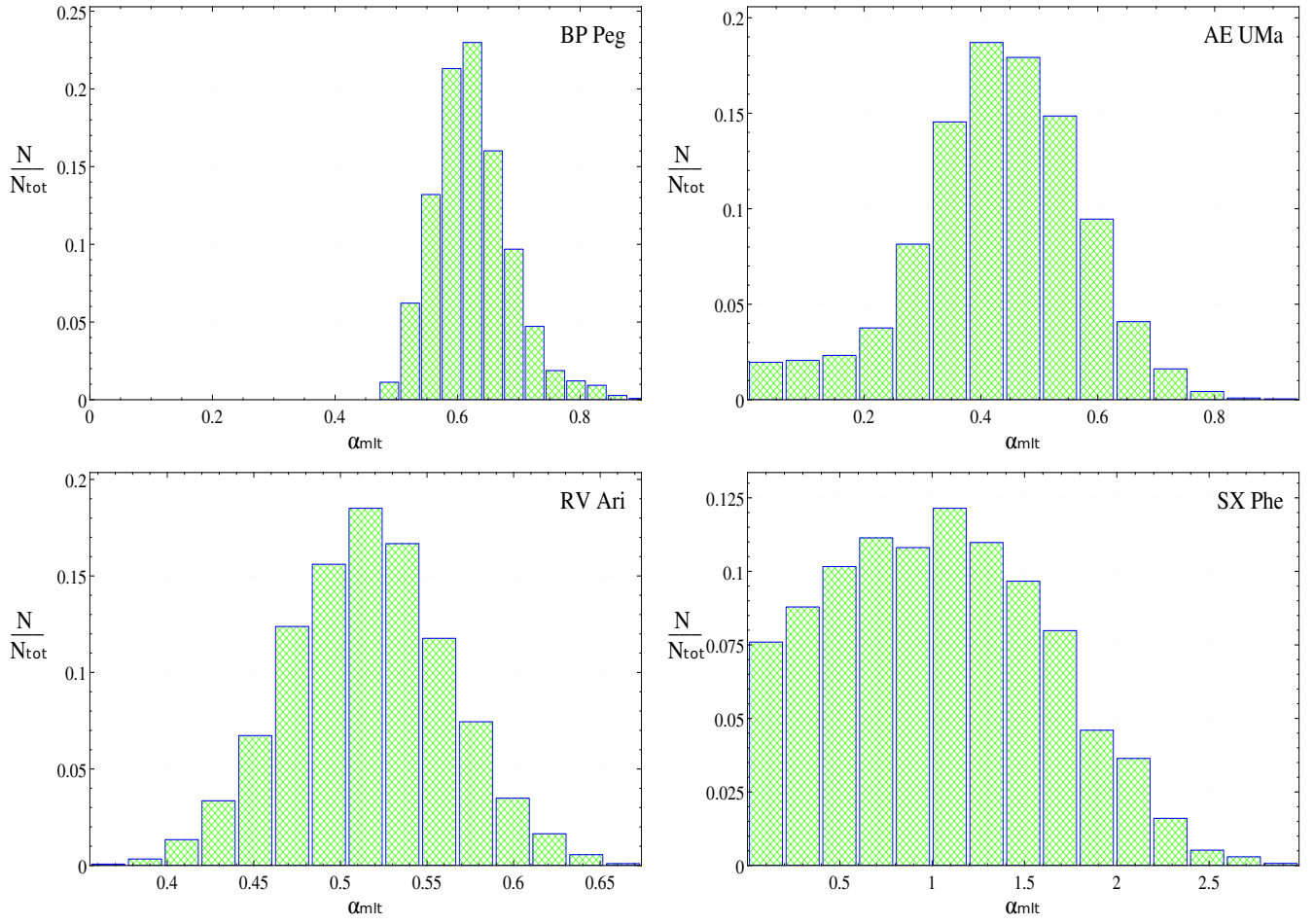


Figure 8. The normalized histograms for the mixing length parameter α_{MLT} for seismic models computed with the OPAL opacities.